ECI 8th International Conference on Boiling and Condensation Heat Transfer
Ecole Polytechnique Fédérale de Lausanne, 3-7 June 2012
Lausanne, Switzerland

EFFECTS OF TURBULENCE AND LONGITUDINAL VORTICES ON VAPOR DISTRIBUTION AND HEAT FLUXES IN SUBCOOLED FLOW BOILING

Gregor Bloch *, Jürgen Loth, Moritz Bruder, Thomas Sattelmayer
*Author for correspondence
Lehrstuhl für Thermodynamik
Technische Universität München
Boltzmannstraße 15
85748 Garching bei München
Email: bloch@td.mw.tum.de

ABSTRACT

Flow boiling experiments were conducted at the transition from nucleate to film boiling to investigate the influence of additional turbulence and longitudinal vortices on critical heat flux (CHF). A low boiling fluoroketone was used as working fluid. Turbulence or vortices were induced using a single-hole orifice or a twisted tape insert. High speed videometry and Particle Image Velocimetry were used to determine the flow parameters and vapor distributions in the channel. Optical probes were applied to obtain point measurements in the bulk of the vapor flow. At CHF, large vapor agglomerations were observed to occur at constant frequencies even with different inserts. In the wake of the agglomerations, gaps in the vapor structure could be seen, for which the PIV measurements showed increased velocities towards the heater surface. The vapor structures and distributions are discussed for different positions and methods of measurement.

BACKGROUND AND MOTIVATION

One of the most interesting and technically relevant phenomena in boiling processes is the transition from nucleate boiling to film boiling, as the abrupt reduction in heat transfer forms a limitation for the safe and effective operation of the heat transferring equipment. Thus a vast number of research projects have been conducted over the last decades with the aim of providing more detailed insight into the effects leading up to the critical heat flux (CHF). Numerous empirical correlations have been proposed, but are often restricted to the systems from which they were derived (Collier and Thome (1994)). For a more general application, mechanistic models have been proposed that base CHF estimation primarily on describable physical phenomena, thus promising greater overall validity and are furthermore better suited for implementation into CFD-codes. Several models have been proposed over the last twenty years that use only few or no empirical constants at all, and have been shown to provide accurate correlations for a variety of geometries and fluids. However, the models still vary strongly in the assumed mechanisms of CHF, and the actual mechanisms of CHF still remain to be understood. Reviews of the models have been given for example by Gersey and Mudawar (1995), Celata and Mariani (1999) and Kandlikar (2001). In the following paragraph, the three most recent and widely used mechanistic CHF models shall be introduced and discussed. The *near wall bubble crowding* was first proposed by Hebel et al. (1981; 1982), and further developed by Weisman and Pei (1983), Ying and Weisman (1986), Lim and Weisman (1990) and Weisman et al. (1994). This model assumes the loss of quenching and subsequent CHF to be caused by a rising concentration of bubbles near the heater surface, which block off the liquid access. It has been commented by a number of researchers (Lee and Mudawar, 1988; Celata et al., 1994b; Celata and Mariani, 1999; Zhang et al., 2004) that a weakness of the model lies in the assumption of CHF to occur at a certain critical void fraction of 82 % (Weisman and Pei, 1983), which however was observed to vary widely for differing mass fluxes and subcoolings by Styrikovich et al. (1970). A slightly newer model is the *sublayer dryout model* which was first introduced by Haramura and Katto (1983) and further expanded by Lee and Mudawar (1988) and which has received increased attention over the last twenty years (Katto, 1990a,b; Celata et al., 1994b, 1995). According to this model, CHF occurs when a liquid sublayer present under the vapor bubbles during nucleate boiling cannot be replenished from the bulk flow any more and evaporates, creating a dry spot on the heater surface. This model was primarily developed for pressures of more than 5 MPa, but was also expanded for lower pressure systems by Katto (1992). Celata et al. (1994b) provided a rationalization of the model, wich enabled the exclusion of empirical constants. It was further expanded by Celata et al. (1995) for cases with non-uniform heating and swirl flow. The swirl was accounted for by modifying the friction factor. The model was further enhanced by Celata et al. (1999) with the *superheated layer vapour replenishment model*, which is based on the sublayer dryout model. This model assumes a liquid layer at saturation temperature (superheated layer) close to the heater surface, which dries out at CHF and is replenished by a vapor blanket. Another recent model is the *interfacial lift-off model* first proposed by Galloway and Mudawar

(1993a,b). Here the loss of so called wetting fronts between coalesced vapor slugs and the subsequent departure of the interface from the heater surface are assumed to be the principal phenomenon leading to CHF. This model was further developed by Gersey and Mudawar (1995) and Zhang et al. (2004, 2007). Only few researchers have commented on the influence of turbulence and secondary flows on the mechanisms leading to CHF. In this report, a number of observations from boiling experiments under the influence of added turbulence and secondary flows is presented and discussed with regard to the presented mechanistic models.

EXPERIMENTAL SETUP

The setup used in the experiments reported here consists of a fluid loop with a rectangular boiling chamber orientated vertically with flow direction upwards. The boiling test rig is shown schematically in fig. 1. The fluid is pumped through a preheater for setting of the subcooling, then enters the main boiling chamber. Inserts for added turbulence and secondary flow structures can be placed at the inlet of the boiling chamber. The main boiling chamber is an improved version of the setup described by Maurus et al. (Maurus, 2003; Maurus et al., 2004; Maurus and Sattelmayer, 2006) with a length of 500 mm and a square inner section of 40x40 mm^2. Heating is done via a 20x200 mm^2 copper bar flush mounted in one of the walls, beginning at 75 mm above the inlet. The copper heater is equipped with 12 cartridge heaters. To measure surface temperature and heat flux, 3 rows of 4 thermocouples are inserted at three different heights along the heater. From the temperature gradients measured by the thermocouples, heat flux can be calculated using Fourier's law, and surface temperature via a polynomic extrapolation. After the boiling chamber, the fluid is cooled down with a double-pipe counterflow heat exchanger, and returned to the pump. A reflux condenser at the highest point keeps the setup open to the atmosphere. A filter and degassing unit can be inserted to remove particles or inert gases from the fluid. As working fluid dodekafluoromethypentanone, available as 3M^{TM} Novec649^{TM} is used. This fluid is chemically and physically similar to the well known FC 72, with a boiling point of 49 °C at ambient pressure and enthalpy of vaporization of 88 kJ/kg. To avoid errors due to possible changes in the heater surface due to cavitation, oxidation, fouling etc., reference measurements at given parameters were conducted after every third experiment. If necessary, the heater was then taken out of the channel and polished. Like this, error bars of 6 % for the heat fluxes and 10 % for the wall superheats were feasible.

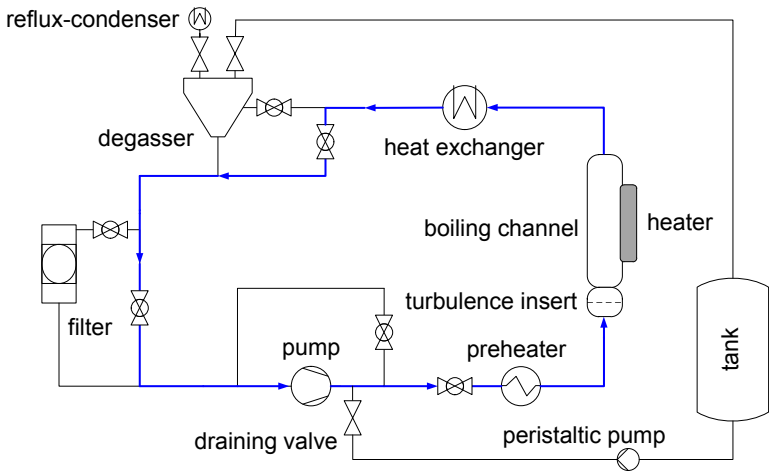

Figure 1: Schematic setup of the boiling loop

FLOW INSERTS

The topic of this work is the study of the effects of secondary flows on the boiling process and the flow regimes near the heater surface. A number of studies have been conducted with inserts stretching along the whole length of the channel, most notably with twisted tapes or coiled wires (Celata et al., 1994a; Weisman et al., 1994; Akhavan-Behabadi et al., 2009). For practical applications such as the rod bundles of pressurized water reactors, a creation of turbulence only at the inlet or at discrete positions is applicable, as seen in the spacer grids of nuclear reactors. This results in a decay of the created secondary flows downstream of the inserts. To account for such effects, turbulence or vortex inducing inserts were only placed at the inlet of the boiling chamber in the setup used for this report. Two kinds of inserts were used in the experiments discussed in this report: first, a simple orifice plate with one hole ($d = 25\,mm$, $\varepsilon = 0.3$) to create strong turbulence and a twisted tape insert with total length of 50 mm and a width of 35 mm, twisted by an angle of 90°. CAD-drawings of the inserts are shown in fig. 2. The decay of turbulence for the single-hole plate was already discussed in Bloch et al. (2011), where an exponential decay of turbulence intensity along the channel was observed. The twisted tape creates a stationary vortex that decayed persited rather long along the channel, with vorticity being still at approx. 70 % of the inlet value after 10 diameters.

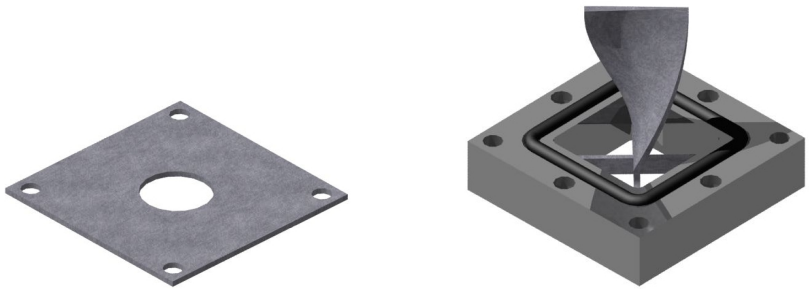

Figure 2: Turbulence inserts used in the experiments, left: single-hole plate, right: twisted tape.

PIV SETUP

A highspeed PIV setup was used to analyze the two-phase flow pattern during boiling. The camera was a Photron Fastcam SA5 which was run at a framerate of 7000 fps and a resolution of 1024x1024 pixel. The lasers used were two Nd:YLF Pegasus lasers by New Wave research inc. with a wavelength of 532 nm. The minimum pulse length of the lasers was ≤ 120 ns and the minimum shutter speed of the camera was 1 μs. For the experiments discussed here, the shutter speed was 1/7000 s, which was fast enough to record pictures without motion blur. The lens used was a Nikon Nikkor lens with a focal length of 200 mm and maximum aperture opening of f/4. In the experiments, the aperture was set between f/8 and f/16. Extension tubes were used to reduce the minimum distance from the image plane, and a polarizing filter was used to reduce errors from reflections at the heater surface and at the interfacial areas. The tracer particles were silver coated hollow glas spheres (S-HGS) by Dantec Dynamics with a mean diameter of 20 μm. The particle density was close enough to the fluid density to be able to neglect errors due to buoyancy. The area observed with PIV was of 25x25 mm^2 size.

OPTICAL PROBES

An important parameter in boiling research is the value of the void fraction present in the channel. A large variety of measurement methods exist, of which many integrate over a line or certain volume (e.g. gamma ray densitometry, photographic methods). To give an accurate measurement of the flow regimes present especially near CHF and thus at high void fractions, a measurement system enabling an aquisition of void fraction within a very small area, ideally a single point is desirable. Such measurements can be realized with the implemention of needle probes, which offer precise and time resolved measurements that require little additional interpretation and post processing. The most common type of needle probes is the electric conductivity needle probe, however as the fluid used in this report was not electrically conductive, the approach via an optical probe was taken. Optical needle probes have already been used in a number of experiments in the past, see e.g. Cartellier and Barrau (1998), Cartellier (1990), Vejrazka et al. (2010). Different types of optical probes have been described, of which the most recent one is the so called mono fiber optical probe, which was also used here. The probe consisted primarily of an optical fiber with a 200 μm silica core and a conically polished tip with an angle of 45°. Laser light at 650 nm was coupled into the fiber at the end and depending on the refractive index surrounding the tip was either reflected back into the fibre or exited into the channel. With a semi-permeable mirror plus necessary additional optical setup, the intensity of the reflected light could be measured with a photodiode and recorded via a computer system. The optical setup is shown in fig. 3. The minimum bubble diameter detectable with the probes was approx. 2 times the diameter of the probe, i.e. 400μm. The fibers were mounted in a stainless steel capillary tube with an outer diameter of

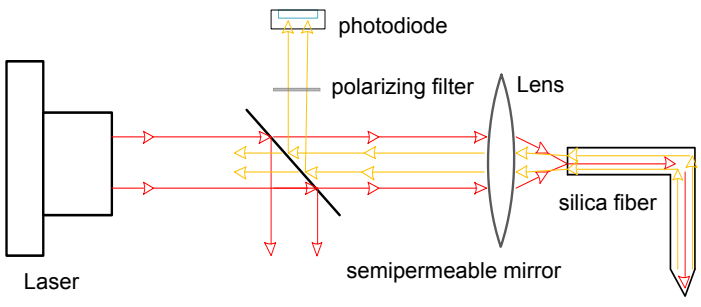

Figure 3: Setup of the beams for the optical probe

1.2 mm for mechanical support, with the fiber protruding ca. 2 mm over the tube. Three fibers were mounted axially movable into the channel at an angle of 30 degrees. Pictures of the optical setup and the fibers in the channel are shown in fig. 4. This setup allowed to measure the number of bubbles and thus the local void fraction at the tip of the fibers. By axially moving the fibers, void fraction profiles at different distances from the heater could be recorded. The measurement rates for the fibers used in this report

ranged from 0.5 to 3 kHz, typically 1 kHz was used. The measured voltage signal was then binarized using a phase determination function (PDF) setting a threshold for bubble detection. A moving average function over 1 s of measurement was used to determine the mean void fraction at the probe tips.

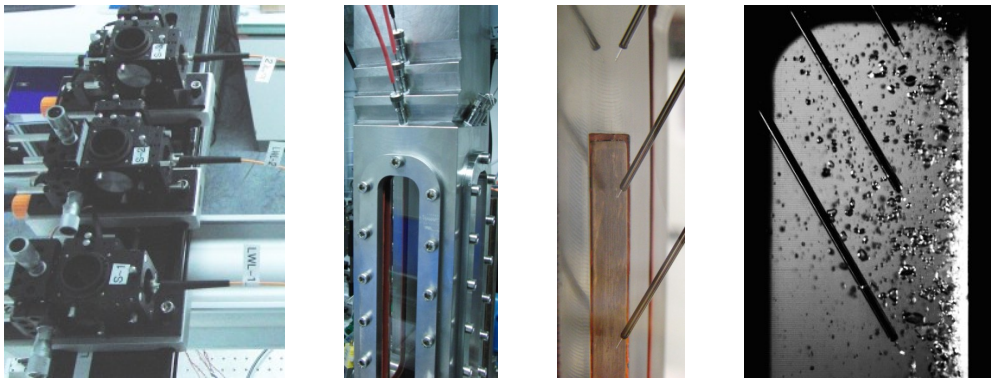

Figure 4: Setup for the optical needle probes. Left to right: optical assemblies housing laser, beam splitter and photodiode for each probe, mounting of three probes (vertical configuration) in the channel, probes inside the channel without heating, probes in boiling flow.

GENERAL OBSERVATIONS ON THE FLOW REGIMES

Flow boiling regimes along the whole boiling curve, up to fully developed film boiling were analyzed. Following the definitions of Galloway and Mudawar (1993b), the regimes will be denoted as follows: after onset of boiling, a *discrete bubble regime* was observed, consisting mainly of isolated single bubbles. At higher wall superheats up to critical heat flux, the bubbles started to merge, forming the *coalescent bubble regime* consisting of smaller single bubbles and large, coalesced bubbles, which moved along the heater at significantly higher velocities than the single bubbles. Near CHF, Galloway and Mudawar (1993b) reported a continuous *wavy vapor layer regime*, which only allowed access to the heater surface at periodically apperaring wetting fronts. A similar regime was observed here, however not consisting of a continuous vapor wave, but rather larger slugs or clots of coalesced bubbles. These appeared periodically and also entailed gaps of low vapor concentration where fresh liquid could reach the heater surface. This regime will further be denoted as *highly coalesced bubble regime*. A visualization of this regime at wall superheat 1 K from CHF is shown in fig. 5 for the empty channel and single hole insert. Only after passing CHF, a continuous layer of vapor on the heater surface was observed, with smaller slugs moving inside the vapor. With added turbulence, as seen in fig. 5, bubbles were dispersed far into the channel. This was observed strongly with the single-hole insert for both nucleate and film boiling, and similarly but less pronounced for the twisted tape.

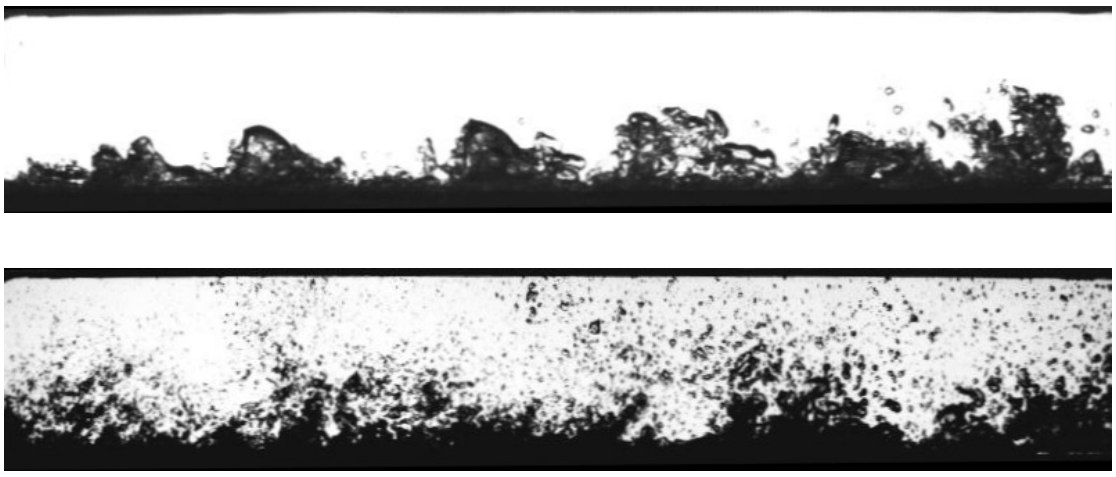

Figure 5: Flow regimes close to CHF for channel without inserts and with single-hole plate.

VAPOR DISTRIBUTION

To gain general insight into the distribution of gas bubbles in the channel, videos at a resolution of 1280x720 pixel and a frame rate of 30 fps were taken over the whole channel length using a Casio Exilim digital camera. The channel was illuminated from the background using an opaque screen and a halogen floodlight. Due to the high speed of the bubbles, tracking of single bubbles was not possible with this setup, but over the recording time of 1 min per measurement, good statistic values could be obtained. The steps taken for the videometric evaluation are shown in fig. 6. The resulting 1800 pictures (1) were first binarized (2), then an algorithm for filling bubble-like structures was applied (3) and finally the average value for every pixel over all images was calculated. Lines of constant integrated intensity were added, showing at which points more than 90, 70, 50, 30, or 10 percent of bubbles were observed. The results clearly showed the better distribution for the case with the single-hole insert, as well as the significantly lower amounts of vapor in film boiling.

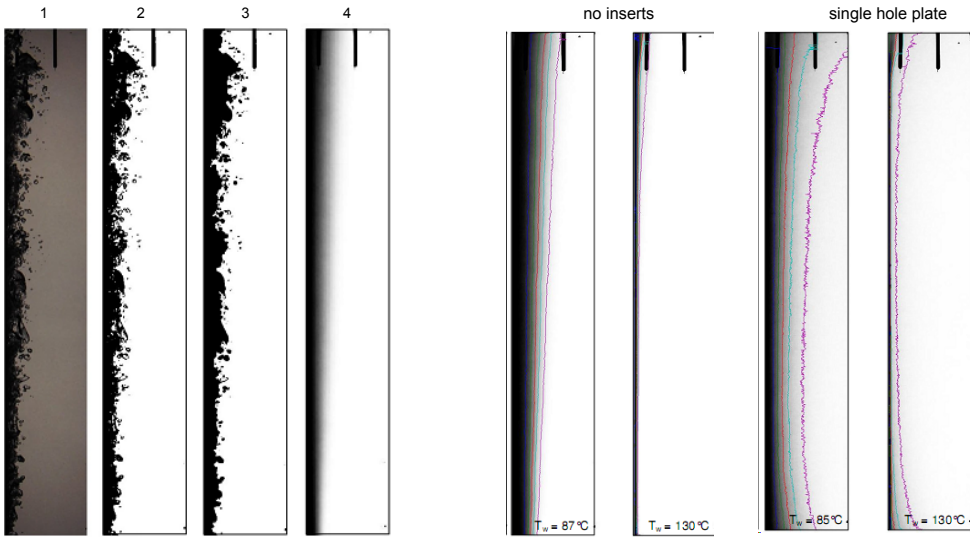

Figure 6: left: processing steps taken for the videometric analysis, right: resulting averaged gas distribution at CHF and in film boiling for channel without inserts and with single-hole plate.

FREQUENCY OF VAPOR SLUGS

In the highly coalesced bubble regime, vapor slugs could be observed at regular intervals. These slugs had average sizes of 15 mm for the case without inserts and 9 mm for the twisted tape insert. For the single-hole plate, the vapor agglomerations were less pronounced as turbulent mixing led to far smaller bubbles, as seen in fig. 5. However, slug-like agglomerations could still be observed, reaching roughly 8 mm into the channel. Behind the slugs, gaps in the vapor structure could be observed similarly to the wetting fronts described by Galloway and Mudawar Galloway and Mudawar (1993b,a). These gaps had a spatial strech of 2-3.5 mm. To measure the frequency of the slugs, high-speed images were binarized and mean intensity for each row calculated (see fig. 7). Due to the assumption of threshold for binarization and filtering of particles from the images, the method is rather rough and does not allow for a precise definition of parameters such as slug length or volume. However, the resulting peaks give a clear measurement of the absolute number of slugs passing the channel. A signal analysis using Fast Fourier Transformation (FFT) was used to to determine the frequency of the vapor slugs, as shown in fig. 7 (right hand side). To determine the average velocity of the slugs, a cross-correlation algorithm was used on the measured intensities for rows of 20 pixel distance. For each insert, a total of 10.000 pictures taken at a frame rate of 7000 fps were evaluated. The experiments were also conducted at a subcooling of 9 K and flow velocity of 0.6 m/s. For the channel without inserts, the plotted mean intensity for the first row of pixels is shown in fig. 7. For the channel without inserts and the twisted tapes, a slug frequency of approx. 25-26 Hz was observed, for the single-hole plate the measured frequency was somewhat lower at approx. 17 Hz. It has to be noted however, that for this insert the method of determination was prone to errors due to the strong distribution of vapor along the channel which prohibited smaller slugs from being detected. Still, as it could also be observed visually, fewer slugs were in fact present. This could be attributed to the better distribution of vapor in the channel, which left less bubbles to coalesce near the heater. It has to be noted that the slugs did not consist solely of a single large vapor bubble, but more of a multitude of smaller, more or less coalesced bubbles and entrained liquid. This could be observed visually from the high-speed images as well as from the point measurements of the needle probes, which detected the slugs as a sequence of multiple short signals instead of a single longer signal as would be received for a single bubble. The avergage vertical velocity of the slugs was measured via cross correlation to be approx. 1 m/s for all inserts, which was significantly faster than the mean flow velocity of 0.6 m/s. The smaller size of the slugs as well as the increased number of bubbles present in the bulk flow confirmed the better distribution of vapor with inserts, most notably for the single-hole plate. The fairly constant frequency of the slugs for all three inserts spawned the assumption that the creation of such agglomerations takes

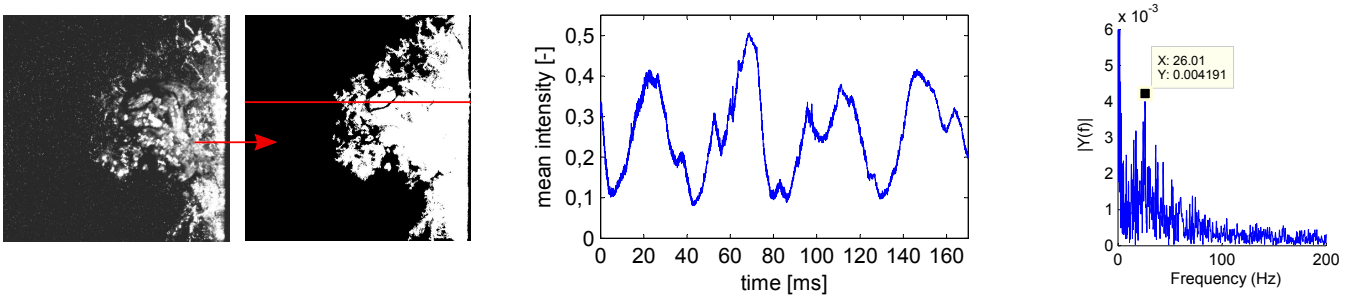

Figure 7: left: Binarization of PIV images, middle: resulting plot of mean intensity over time for first row of pixels. The slug shown on the left corresponds to the peak at 25 ms, right: FFT for detection of slug frequency.

place in a region of the boundary layer that is not affected by the secondary flows due to vapor blockage. This could be further substantiated by the PIV measurements (see p. 7).

COMPARISON OF TRANSIENT AND STEADY-STATE EXPERIMENTS

Boiling experiments were carried out with transient and steady state heating. With transient heating, the whole test rig was at room temperature when starting the experiment and the electrical power to the heater was kept constant at 2,2 kW. This mode allowed to measure a whole boiling curve for set parameters within ca. 30 min, plus 2-3 hours for cooling down afterwards. Like this, a large database could be created at moderate time effort. However due to the inertia of the used copper heater the measured heat fluxes may be subject to larger errors at fast transients. Therefore, steady state measurements were conducted to allow a comparison of the heat fluxes to the ones measured in the transient experiments. For these experiments, fluid subcooling was kept constant at 9 K, and the electrical power to the heater was varied. Steady state was assumed when the wall temperatue fluctuations were not higher than the errors of the thermocouples. For the steady state measurements, the heat fluxes were averaged over 1 min of measurement. A comparison of the heat fluxes measured for steady and transient states are shown in fig. 8. Before the onset of boiling (wall superheat ≤ 8 K), steady state heat fluxes were smaller due to the high temporal change in temperature. At higher wall superheat, only little differences were observed. As critical heat flux is obviously difficult to reach at steady state, a wall temperature of 1 K below CHF was set as the highest pre-CHF value. Here, the average values were 7.4 % lower than CHF in the transient case. The critical heat fluxes measured for the transient case at subcooling of 9 K and flow velocity of 0.6 m/s were

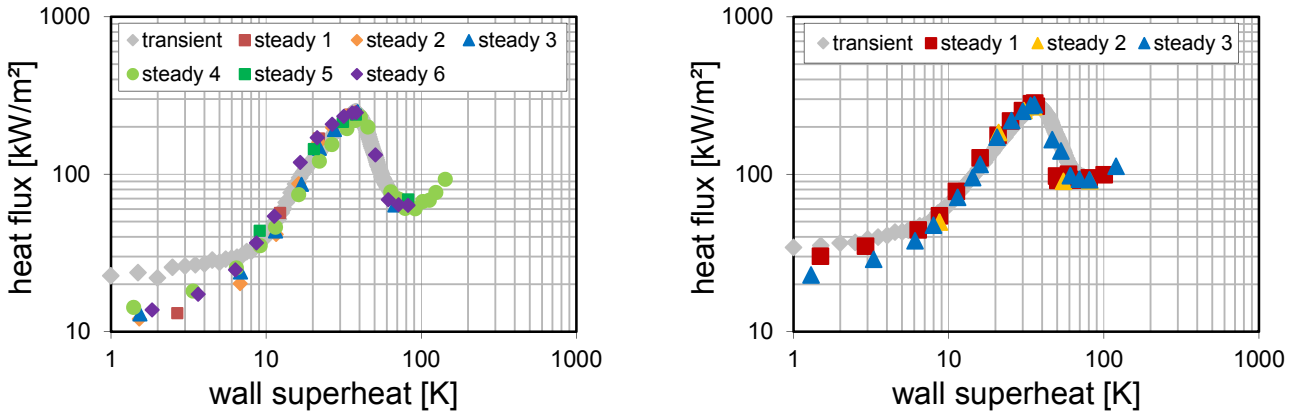

Figure 8: Heat fluxes for transient and steady state experiments, left: empty channel, right: single-hole plate.

260 kW/m^2 for the empty channel and 285 kW/m^2 for the single-hole plate. This was an increase of 9 % overall critical heat flux. At a subcooling of 27 K however, the increase in CHF was significantly higher at 20 %, with absolute CHF values of 327 kW/m^2 for the empty channel and 393 kW/m^2 for the orifice. The twisted tape yielded only marginal increases in CHF for this flow rate. Measurement of void fraction for steady state and transient case gave similar results as the heat fluxes. Fig. 9 shows the measured void fractions for needle probes at the upper end of the heater with a distance of 4 mm from the heater surface. The steam film after CHF is very thin and does not reach far into the channel, so that void fraction is measured as zero after CHF. The values measured for steady state conditions were approximately identical to the steady state values. Shown on the right hand side in fig. 9 are the curves for void fraction and heater surface temperature over time, clearly showing the rise in void fraction at the onset of boiling, which can also be seen from the smaller slope of the temperature, and the decrease of void fraction and excursion of temperature at

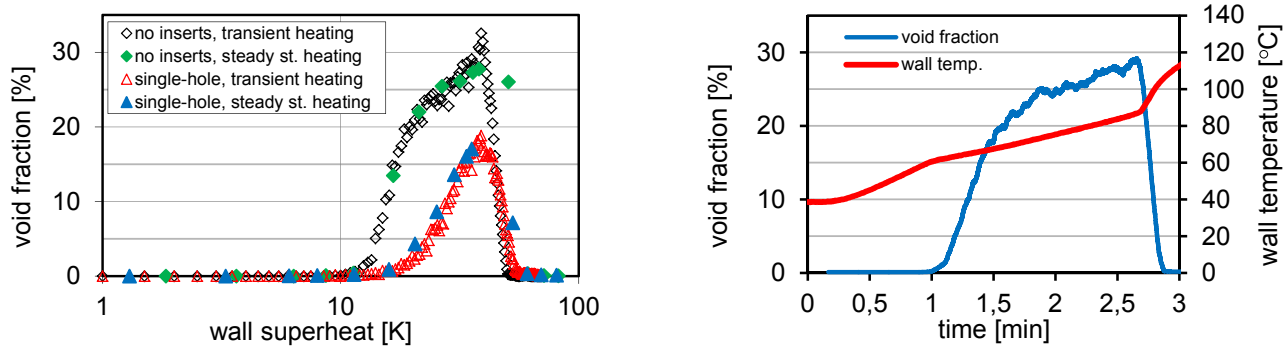

Figure 9: left: Void fraction measured with optical needle probes for transient and steady state experiments, right: void fraction and wall temperature for channel without inserts for transient heating over time.

CHF. From these results, it could be concluded that the transient mode of running the experiments had only little influence on the measured heat fluxes, especially in regions close to CHF.

VAPOR DISTRIBUTION NEAR THE HEATER SURFACE

Void fraction measurements were also conduted with an optical probe at different distances to the wall. Here, the probe was mounted axially moveable at an angle of 30° to the wall. At the beginning of each measurement, the probe distance to the wall was approx. 0.1 mm, and the probe was moved backwards stepwise during the experiment. Measurements were conducted for the channel without inserts and with the single-hole plate for flow regimes of fully developed nucleate boiling 1 K from CHF and during film boiling. In all cases the wall temperatures were steady state and liquid flow velocity of 0.6 m/s. Void fractions were averaged over 1 min of measurement for each data point. Fig. 10 shows the measured void fractions for nucleate boiling near CHF and film boiling. In nucleate boiling, maximum values of 57 % were measured for the case without inserts and 52 % for the

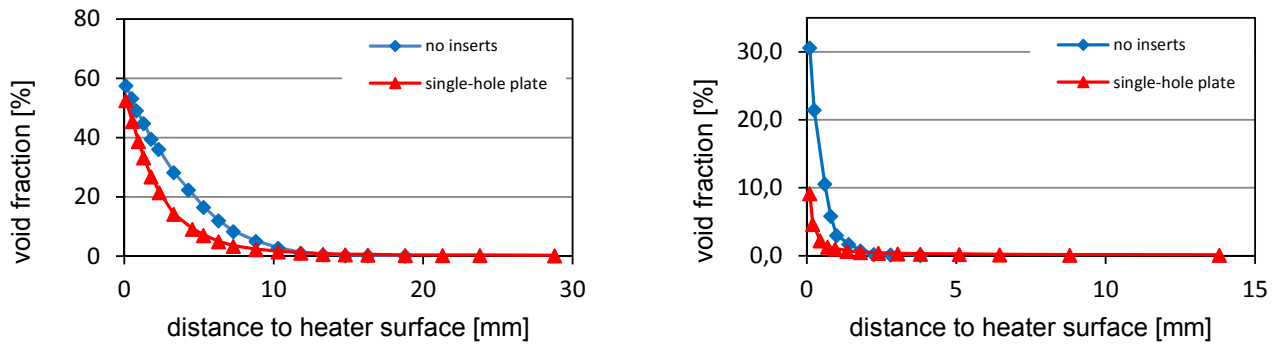

Figure 10: Distribution of void fraction near the heated wall for fully developed nucleate boiling close to CHF (left) and fully developed film boiling (right).

single-hole plate. Again, this showed the better distribution of vapor in the channel for the case with added turbulence. As the probe was still a macroscopic distance away from the heater surface, the void fraction at CHF could not be determined without uncertainty. However, the values were clearly below the 82 % proposed for the so called bubbly layer near the wall in the bubble crowding model Weisman and Pei (1983). At film boiling, the measured values were 31 % and 9 %. The probe did not enter the vapor film as the film thickness was below the 0.1 mm distance from the tip to the heater, thus the measured void fractions show the amount of smaller bubbles that were carried out from the vapor film. At larger distances to the heater, slightly higher void fractions were observed for the single-hole plate due to the better distribution of vapor.

PIV RESULTS

The PIV measurements were conducted for three different boiling regimes: discrete bubble regime at wall temperature of 57 K, highly coalesced bubble regime at $T_{wall} = 87$ K and steady state film boiling at a wall temperature of 130 K. The fluid velocity was kept constant at 0.6 m/s, subcooling was 9 K. In the discrete bubble regime and film boiling only small horizontal components and no significant bubble wakes could be observed for all inserts. For the single-hole insert, fluctuations in horizontal velocity in the range of ±200% of the mean vertical velocity were observed, which explained the higher heat fluxes observed with this insert. For the twisted tape, the vortice could be observed to create horizontal velocities of 0.2 m/s, but did not reach up to the heater surface.

For the highly coalesced regime, the large number of bubbles were observed to block the heater surface from the bulk flow. The velocity fluctuations added via the inserts were absorbed in the outer layers of the bubble structure, which led to a better vapor distribution but failed to affect the heater surface itself. Also, as discussed above, large vapor agglomerations were observed at certain frequencies. In the wake of these agglomerations/slugs, two interesting phenomena could be observed: firstly, gaps in the vapor structure were observed with length of 2-3.5 mm as discussed above. Secondly, the velocities in the wake showed a strong orientation towards the heater surface, with horizontal velocities of 0.16 to 0.23 m/s towards the heater even for the channel without inserts. The absolute vector field for a vapor slug is shown on the left of fig. 11, and for better visualization of the horizontal components with subtracted mean vertical velocity on the right. These observations seem to support the findings of Galloway and

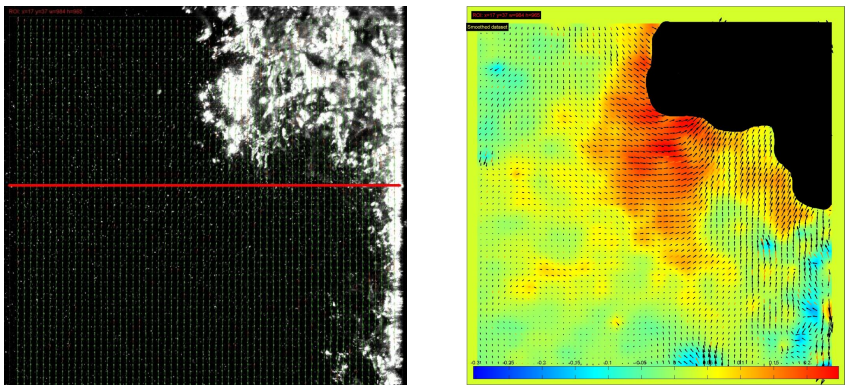

Figure 11: Bubble clot with corresponding vector field (left), vector field with average vertical velocity subtracted (right), colorbar shows vector length

Mudawar, assuming the wetting and cooling of the heater surface in the gaps behind agglomerations to be the main mode of heat transfer close to CHF. It would appear logical from these results that a further shortening of the vapor gaps might indeed be the critical mechanism for CHF.

SUMMARY AND OUTLOOK

Subcooled boiling and the corresponding two-phase flow patterns under the influence of turbulence or a longitudinal vortex were analyzed for different flow inserts at the channel inlet. An enhanced distribution of vapor bubbles over the channel cross-section was observed even in the discrete bubble regime shortly after ONB, most notably with the single-hole orifice plate. Vapor distribution was analyzed both from videometric analyses and from optical probe measurements. At higher heat fluxes, strongly coalescent bubbles were observed to form slug-like structures of vapor clots, that moved significantly faster than the single bubbles and the mean flow. The slugs appeared at frequencies of around 25 Hz for cases with and without inserts, which led to the assumption that the formation of slugs takes place in a region close to the wall that is isolated from secondary flow effects by surrounding bubbles. In fact, as seen by PIV measurements, effects of slug wakes proved to be greater than the velocity fluctuations induced by the inserts. Also, results from the optical probes showed that the void fraction close to the heater varied only slightly with added turbulence, while considerably larger differences could be observed in the bulk flow. From this, it could be concluded that added secondary flows, even with high turbulence intensities, generally have only limited influence on vapor formation at the heater surface in boiling regimes close to CHF. This was also assumed to be the reason for the decreasing influence of turbulence on the heat flux with decreasing subcooling. At higher subcooling, more and larger bubbles are present, which leads to an increased isolation of the heater from the bulk flow. This would support the first assumptions of the bubble crowding model. However, as heat flux measurements still showed a strong increase of CHF with added turbulence, secondary flows obviously had an influence on the heat transfer. A very likely mechanism for this might be found in the wetting fronts behind the vapor agglomerations also described by Galloway and Mudawar (1993b,a) in their interfacial lift-off model. The PIV measurements showed horizontal components at values of up to 30 % of the vertical flow velocity for cases without added turbulence. With the single-hole plate, horizontal fluctuations of up to 200 % of the vertical flow velocity were observed. Coupled with the added mixing in the bulk liquid, the present secondary flows can be expected to have a strong impact on the quenching effect taking place in a wetting front. However, as liquid subcooling decreases, the temperature difference of liquid from the bulk to the liquid near the heater is smaller and thus the quenching effects by added turbulence are also reduced. The transition to film boiling could not be observed by PIV and/or videometry for the experiments discussed here, as the process was too slow for the possible recording times. Still, it could be stated that a likely mechanism lies in the closing of the vapor gaps with increasing vapor holdup, which finally leads to an isolation of the heater surface. For future experiments, a variation of the experimental parameters is intended, especially to gain more insight into the influence of subcooling and flow rate on the vapor structures. As the steady state measurements showed only little difference to transient heating, the following experiments shall be conducted primarily in transient mode to create a larger database. As the transition process into film boiling is of particular interest, further experiments using optical needle probes and high speed videometry shall be conducted for the transient.

ACKNOWLEDGEMENT

The authors are grateful for the financial support by the Bundesministerium für Bildung und Forschung (BMBF) who funded the research project under the project number 02NUK010E.

REFERENCES

Akhavan-Behabadi, M. A.; Kumar, Ravi, and Jamali, M., (**2009**). Investigation on Heat Transfer and Pressure Drop During Swirl Flow Boiling of R-134a in a Horizontal Tube. *International Journal of Heat and Mass Transfer*, 52:1918–1927.

Bloch, G.; Schmitt, D., and Sattelmayer, T., (**2011**). Influence of Turbulence Induced by Perforated Plates on Heat Transfer and Critical Heat Flux in Subcooled Flow Boiling. In *Proceedings of ITP-2011*, Dresden, Germany.

Cartellier, A., (**1990**). Optical Probes for Local Void Fraction Measurements:Charakterisation of Performance. *Review of Scientific Instruments*, 61:874–886.

Cartellier, A. and Barrau, E., (**1998**). Monofiber Optical Probes for gas Detection and gas Velocity Measurements: Conical Probes. *International Journal of Multiphase Flow*, 24:1265–981294.

Celata, G. P.; Cumo, M., and Mariani, A., (**1994a**). Enhancement of CHF Water Subcooled Flow Boiling in Tubes Using Helically Coiled Wires. *Int. J. Heat Mass Transfer*, 37:53–67.

Celata, G. P.; Cumo, M.; Mariani, A.; Simoncini, M., and Zummo, G., (**1994b**). Rationalization of Existing Mechanistic Models for the Prediction of Water Subcooled Flow Boiling Critical Heat Flux. *Int. J. Heat Mass Transfer*, 37:347–360.

Celata, G. P.; Cumo, M.; Katto, Y., and Mariani, A., (**1999**). Prediction of the Critical Heat Flux in Water Subcooled Flow Boiling Using a new Mechanistic Approach. *International Journal of Heat and Mass Transfer*, 42:1457–1466.

Celata, G.P. and Mariani, A., (**1999**). CHF and Post-CHF (Post-Dryout) Heat Transfer, Chapter 17. *Handbook of Phase Change: Boiling and Condensation, edited by Kandlikar, S.G. and Shoji, M. and Dhir, V.K.*, pages 443–493.

Celata, G.P.; Cumo, M.; Mariani, A., and Zummo, G., (**1995**). The Prediction of the Critical Heat Flux in Water-Subcooled Flow Boiling. *Int. J. Heat Mass Transfer*, 38:1111–1119.

Collier, John G. and Thome, John R. (**1994**), *Convective Boiling and Condensation*. Oxford University Press, third edition.

Galloway, J. and Mudawar, I., (**1993a**). CHF Mechanism in Flow Boiling From a Short Heated Wall - I. Examination of Near-Wall Conditions With the aid of Photomicrography and High-Speed Video Imaging. *Int. J. Heat Mass Transfer*, 36:2511–2526.

Galloway, J.E. and Mudawar, I., (**1993b**). CHF Mechanism in Flow Boiling From a Short Heated Wall - II. Theoretical CHF Model. *Int. J. Heat Mass Transfer*, 36:2527–2540.

Gersey, Christopher O. and Mudawar, Issam, (**1995**). Effects of Heater Length and Orientation on the Trigger Mechanism for Near-Saturated Flow Boiling Critical Heat Flux - II. Critical Heat Flux Model. *lnt. J. Heat Mass Transfer*, 38:643–654.

Haramura, Y. and Katto, Y., (**1983**). A New Hydrodynamic Model of Critical Heat Flux, Applicable Widely to Both Pool and Forced Convection Boiling on Submerged Bodies in Saturated Liquids. *International Journal of Heat and Mass Transfer*, 26: 389–399.

Hebel, W. and Detavernier, W., (**1982**). On the Velocity Profile of Vapour Bubbles at Critical Heat Flux. *Nuclear Engineering and Design*, 74:253–257.

Hebel, W.; Detavernier, W., and Decreton, M., (**1981**). A Contribution to the Hydrodynamics of Boiling Crisis in a Forced Flow of Water. *Nuclear Engineering and Design*, 64:433–445.

Kandlikar, S. G., (**2001**). Critical Heat Flux in Subcooled Flow Boiling - an Assessment of Current Understanding and Future Directions for Research. *Multiphase Science and Technology*, 13:207–232.

Katto, Y., (**1990a**). A Physical Approach to Critical Heat Flux of Subcooled Flow Boiling in Round Tubes. *Int. J. Heat Mass Transfer*, 33:611–620.

Katto, Y., (**1990b**). Prediction of Critical Heat Flux of Subcooled Flow Boiling in Round Tubes. *Int. J. Heat Mass Transfer*, 33: 1921–1928.

Katto, Y., (**1992**). A Prediction Model of Subcooled Water Flow Boiling CHF for Pressure in the Range 0.1-20 MPa. *Int. J. Heat Mass Transfer*, 35:1115–1123.

Lee, C. H. and Mudawar, I., (**1988**). A Mechanistic Critical Heat Flux Model for Subcooled Flow Boiling Based on Local Bulk Flow Conditions. *Int. J. Multiphase Flow*, 14:711–728.

Lim, J. C. and Weisman, J., (**1990**). A Phenomenologically Based Prediction of the Critical Heat Flux in Channels Containing an Unheated Wall. *Int. J. Heat Mass Transfer*, 33:203–205.

Maurus, R., (**2003**). *Bestimmung des Blasenverhaltens beim unterkühlten Strömungssieden mit der digitalen Bildfolgenanalyse*. PhD thesis, Technische Universität München.

Maurus, Reinhold and Sattelmayer, Thomas, (**2006**). Bubble and Boundary Layer Behavior in Subcooled Flow Boiling. *International Journal of Thermal Science*, 45:257–268.

Maurus, Reinhold; Ilchenko, Volodymyr, and Sattelmayer, Thomas, (**2004**). Automated High-Speed Video Analysis of the Bubble Dynamics in Subcooled Fow Boiling. *International Journal of Heat and Fluid Flow*, 25:149–158.

Styrikovich, M. A.; Nevstrueva, E. I., and Dvorina, G. M., (**1970**). The Effect of Two-Phase Flow Pattern on the Nature of Heat Transfer Crisis in Boiling. In *Heat Transfer 1970, Papers Presented at the Fourth International Heat Transfer Conference, Paris - Versailles 1970*, 1970.

Vejrazka, Jirí; Vecer, Marek; Orvalho, Sandra; Sechet, Philippe; Ruzicka, Marek C., and Cartellier, Alain, (**2010**). Measurement Accuracy of a Mono-Fiber Optical Probe in a Bubbly Flow. *International Journal of Multiphase Flow*, 36:533–548.

Weisman, J. and Pei, B. S., (**1983**). Prediction of Critical Heat Flux in Flow Boiling at low Qualities. *Int. J. Heat Mass Transfer*, 26:1463–1477.

Weisman, J.; Yang, J. Y., and Usman, S., (**1994**). A Phenomenological Model for Boiling Heat Transfer and the Critical Heat Flux in Tubes Containing Twisted Tapes. *Int. J. Heat Mass Transfer*, 37:69–80.

Ying, S. H. and Weisman, J., (**1986**). Prediction of Critical Heat Flux in Flow Boiling at Intermediate Qualities. *Int. J. Heat Mass Transfer*, 29:1639–1648.

Zhang, Hui; Mudawar, Issam, and Hasan, Mohammad M., (**2004**). Investigation of Interfacial Behavior During the Flow Boiling CHF Transient. *International Journal of Heat and Mass Transfer*, 47:1275–1288.

Zhang, Hui; Mudawar, Issam, and Hasan, Mohammad M., (**2007**). Photographic Study of High-Flux Subcooled Flow Boiling and Critical Heat Flux. *International Communications in Heat and Mass Transfer*, 34:653–660.